I&EC research
Industrial & Engineering Chemistry Research

Article

pubs.acs.org/IECR

Effect of Cellulose Crystallinity on Solid/Liquid Phase Reactions Responsible for the Formation of Carbonaceous Residues during Pyrolysis

Zhouhong Wang,[†] Brennan Pecha,[†] Roel J. M. Westerhof,[‡] Sascha R. A. Kersten,[‡] Chun-Zhu Li,[§] Armando G. McDonald,[∥] and Manuel Garcia-Perez*[,†]

[†]Biological Systems Engineering, Washington State University, Pullman, Washington 99164, United States

[‡]Thermo-Chemical Conversion of Biomass Group, Faculty of Science and Technology, University of Twente, Postbus 217, 7500AE Enschede, The Netherlands

[§]Fuels and Energy Technology Institute, Curtin University of Technology, GPO Box U1987, Western Australia, 6845, Australia

[∥]Department of Forest, Rangeland and Fire Sciences, University of Idaho, Moscow, Idaho 83844, United States

ABSTRACT: This study reports changes in solid phase composition when samples of Avicel cellulose (crystallinity: 60.5%) and ball-milled microcrystalline cellulose (crystallinity: 6.5%) were subjected to pyrolysis in a spoon reactor. Solid state chemistry evolution was examined by hydrolysis-ion exchange chromatography, scanning electron miscroscopy (SEM), Fourier transform infrared (FTIR), and ^{13}C nuclear magnetic resonance (NMR). The liquid reaction intermediate was found to cause particle agglomeration at temperatures below 300 °C. At higher temperatures, the ball-milled cellulose melted completely but the more crystalline cellulose conserved its fibrous structure. The formation of C═O and C═C groups was accelerated by the presence of liquid intermediates derived from the amorphous cellulose. The content of cross-linked cellulose was quantified by the combined use of acid hydrolysis and ^{13}C NMR. A new reaction mechanism to describe the changes in the solid residue composition at different reaction conditions is proposed.

1. INTRODUCTION

With the increasing demand of liquid transportation fuel and the gradual depletion of crude oil, the production of fuels and chemicals from lignocellulosic materials continues to gain societal interest. Using lignocellulosic materials for biofuel production has the potential to greatly reduce greenhouse gas production.[1−3] The pyrolysis of lignocellulosic materials followed by the refining of the bio-oil product is one of the most promising alternatives currently studied for the production of transportation biofuels.[4−6]

Cellulose is the most abundant carbohydrate biopolymer in nature and represents approximately 40−45 mass percent in dry wood.[7] During pyrolysis, cellulose degrades into anhydro-saccharides which are considered useful for a variety of applications.[8,9] Pyrolysis of cellobiitol (a disaccharide surrogate) was found early on to produce primarily levoglucosan at higher temperatures and low pressure; however at a lower temperature (171 °C), it was found to undergo intermolecular nucleophilic substitution at the hydroxyl groups to produce large oligosugars.[10] Ponder et al. found that the removal of alkali and alkali earth metal ions and salts by acid washing significantly increased the yield of levoglucosan.[11] However, Richards et al. found that transition metals are actually capable of increasing the yield of levoglucosan.[12]

Pyrolytic anhydro-saccharides (chiefly levoglucosan) can be easily hydrolyzed to obtain glucose or can be directly fermented to obtain ethanol or as a source for chemicals like furans and levulinic acid.[13,14] The formation of these sugars is largely influenced by process conditions like temperature and heating rate.[8] Pyrolysis conditions also affect the structure of the remaining biochar.

Although many researchers have studied cellulose pyrolytic reactions,[15−22] there are few studies on the changes occurring in solid phase.[23] The widely accepted Broido−Shafizadeh pyrolysis reaction scheme considers the formation of active cellulose as the reaction rate limiting step followed by the simultaneous formation of char and volatile compounds.[20,24] Other important reaction schemes include the Waterloo,[25] Diebold,[26] Wooten−Seeman−Hajaligol,[27] and Varhegyi−Antal[28,29] mechanisms. After a thorough review, we found that only a few considered a multistep sequence of solid phase reactions: (i) the Varhegyi−Antal model considers a sequence of reactions responsible for changes in the structure of the carbonaceous residue formed;[28,29] (ii) the Lin model initiates from anhydro-saccharides with degrees of polymerization (Dp) up to 7, followed by the formation of monosaccharide derivatives, followed by furans and char;[17] (iii) Westerhof[30] (biomass) and Lewellen[31] (cellulose) describe a mechanism by which some pyrolysis products are trapped in the particle by mass transfer limitations and henceforth form new compounds, which can either escape from the particle or remain trapped. Eventually, these trapped products can combine to form char.

The role of cellulose crystallinity on pyrolysis reactions has received limited attention.[32−35] As reviewed by Antal,[36] early

Received: May 5, 2013
Revised: January 20, 2014
Accepted: January 27, 2014
Published: January 27, 2014

   dx.doi.org/10.1021/ie4014259 | Ind. Eng. Chem. Res. 2014, 53, 2940−2955

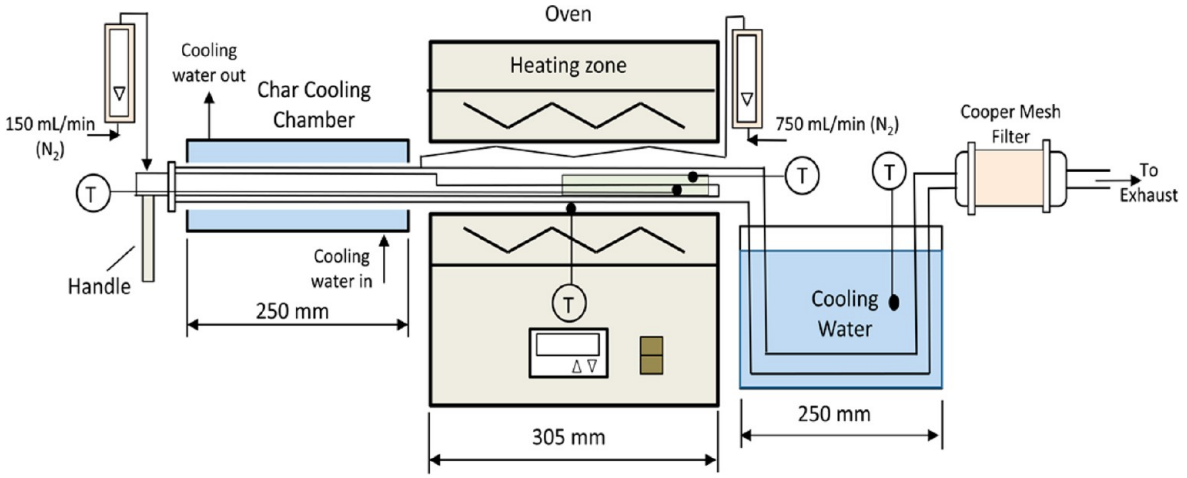

Figure 1. Experimental set up (spoon reactor).

results showed that noncrystalline cellulose (ball-milled or ammonia-swelled cellulose) has a higher weight loss rate than crystalline cellulose.[34,35,37−39] Kilzer and Broido[40] postulated that crystalline cellulose promoted dehydration reactions, and it was proven by Weinstein and Broido[35] that crystalline cellulose produced more char through inter-ring cross-linking reactions. It is also understood that cellulose crystallinity remains constant until weight loss is over 60%, indicating that both crystalline and amorphous cellulose share similar depolymerization reaction.[35,37,38] In addition, Shimazu and Sterling found that amorphous cellulose breaks down at low temperatures.[41] Kato and Kamorita found that, with temperature between 200 and 300 °C, amorphous cellulose produced more furfural and 5-hydroxy-methylfurfural.[42] At temperatures over 500 °C, crystalline cellulose produced more acetaldehyde than amorphous cellulose.[42] Our group has recently found that low cellulose crystallinity does not dramatically change the levoglucosan yield, but it does affect the formation of liquid intermediates.[43]

Among the models so far developed, only the Antal model[44] takes into account the effect of cellulose crystallinity on the formation of carbonaceous solid residues. However, this model does not explicitly consider the formation of liquid intermediates or the formation of cross-linked saccharides. Developing a model that predicts how pyrolysis conditions affect the structure of the biochar product is critical to controlling the production of anhydro-saccharides and the development of biochar based products.

The formation of a liquid intermediate, directly observed by the groups of Professors Lede[45,46] and Dauenhauer,[47] has been found to affect the evolution of carbonaceous materials.[48] The major cellulose pyrolysis product levoglucosan has a boiling point between 304.5 and 340 °C.[48−50] Thus, if not removed fast enough, it can remain in the liquid intermediate phase during pyrolysis and polycondense into char.[51] The formation of this liquid intermediate is also critical for the ejection of heavy products (oligo-saccharides) during the pyrolysis process.[52]

The main goal of this paper is to study the effect of cellulose crystallinity on the formation of liquid intermediates during pyrolysis in a spoon reactor and the reactions responsible for char formation. We also propose a new reaction scheme based on our experimental observations.

2. MATERIALS AND METHODS

2.1. Material. Microcrystalline "control" cellulose (Avicel, PH-101, particle size ∼50 μm, Sigma-Aldrich) was dried.

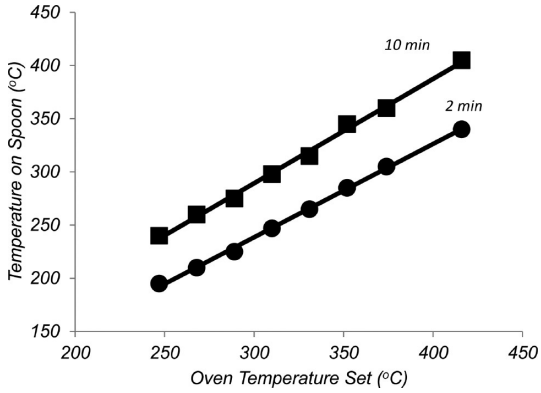

Figure 2. Calibration of spoon temperature (temperature in the spoon at the first 2 min and after reaching equilibrium at 10 min).

Table 1. FTIR Peak Assignments[54−59]

wavenumber (cm^{-1})	peak assignment
895−898	glucose ring stretch, C1—H deformation, C—H deformation in cellulose
990	C—O (secondary alcohols skeletal vibrations)
1020−1050	C—O stretching (C-6 skeletal vibrations)
1050−1070	C—O stretching (C-3 skeletal vibrations)
1080	C—O—C (pyranose ring skeletal vibrations)
1110	C—OH (skeletal vibrations)
1160	C—O—C (antisymmetrical bridge stretching at b-glucosidic linkage)
1200	C—O (stretching in pyranose ring)
1310−1360	OH in plane bending, C—C and C—O (skeletal vibrations)
1372	C—H symmetric deformation
1360	O—H (bending)
1425	CH_2 scissoring
1597−1620	C═C stretching
1694−1710	C═O stretching
2800−3000	C—H stretching
3100−3600	O—H stretching

dx.doi.org/10.1021/ie4014259 | Ind. Eng. Chem. Res. 2014, 53, 2940−2955

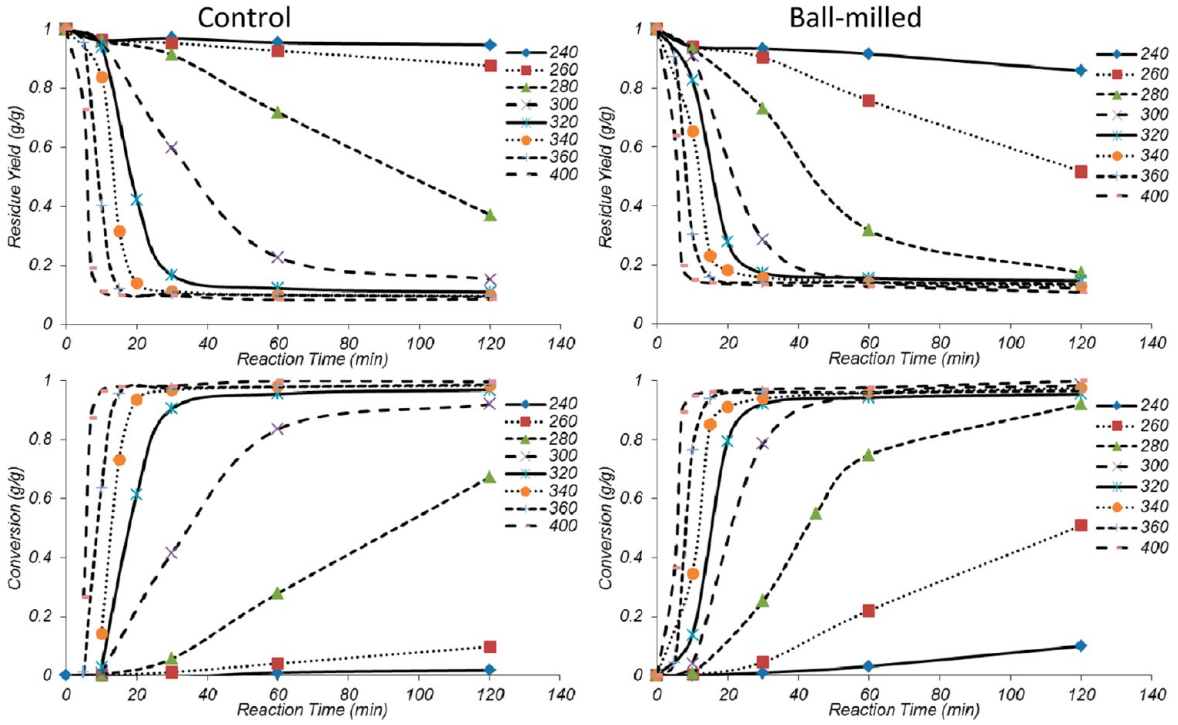

Figure 3. Residue yields from a spoon reactor at different temperatures and reaction time, with control crystalline cellulose on the left and ball-milled cellulose on the right.

Amorphous cellulose was created by ball-milling control cellulose at 300 rpm for 24 h (Across International PQ-N2, ceramic 100 mL jar and balls). The characterization of both samples has been reported elsewhere.[43] Avicel had a crystallinity of 60.5%, and the ball-milled cellulose had a crystallinity of 6.5%. The ash content analysis was carried out with three replicates. The ball-milling introduced alumina ceramic pieces which increased the ash content from values close to the detection limit to 0.58 ± 0.13 wt %.

2.2. Spoon Reactor. A spoon reactor similar to the one described by Mauviel et al. was used for these pyrolysis experiments.[53] Figure 1 shows the scheme of our spoon reactor. It has a char cooling chamber which is utilized for fast cooling of treated samples and for the resting of untreated samples waiting for oxygen removal from the pyrolysis chamber. A Lindberg/Blue 1100 tube furnace (single point) was utilized as the heating source, and a stainless steel tube was used as the heating chamber (18.8 mm i.d., 305 mm in length). Approximately 400 mg of cellulose sample was evenly distributed (by visual estimate) onto a 11 cm long region of the spoon (12.5 mm i.d., 22 cm long half tube) with a thickness of ∼1 mm. The stainless steel spoon was put on a holder and was introduced into a water cooled chamber under nitrogen for 20 min to remove oxygen. The sample was then pushed into a heating chamber (pyrolysis zone) and held at that temperature for a designated time.

The experimental temperature was calibrated by thermocouple (type K, armored and grounded) directly on the spoon at the position where the cellulose sample was heated. The temperature of the spoon was measured at different times. For all the tests conducted, the spoon reached the targeted temperature before 10 min. Figure 2 shows the temperature in the spoon after 2 and 10 min as a function of the temperature in the oven. The linear correlation obtained between the spoon temperature and the temperature of the oven was used as calibration curve for all our experiments.

In the first 2 min the spoon could reach a temperature 45−65 °C lower than the one targeted. The heating rate achieved in the first 2 min was relatively fast (107 °C/min for the samples heated to 250 and 190 °C/min for the samples heated to 400 °C). So our experiments were conducted at heating rate faster than those typically used in slow pyrolysis studies (less than 50 °C/min) but slower than those encountered in fast pyrolysis conditions (hundreds of degrees Celcius per second). A constant nitrogen flow of 900 mL/min at TPN was use to prevent oxidation. Here, 150 mL/min of nitrogen was fed into the char cooling chamber and the rest (750 mL/min) was preheated in the furnace and directed into the reactor. After the experiment, the spoon with residue was pulled back into the cooling chamber and cooled for 15 min to 20 °C. The mass of the solid residue obtained was reported for all the experiments. The term "yield" was defined as the mass of the product of interest divided by mass of the original cellulose.

2.3. Analysis of Solid Residues. *2.3.1. Fourier Transform Infrared (FTIR) Spectroscopy.* The solid residue samples obtained in the spoon reactor were analyzed with a Shimadzu FTIR with attenuated total reflection (ATR, MIRacle equipped with a Ge crystal, PIKE Technology). This method was utilized to monitor the change of functional groups by their peaks at certain wavelengths (see Table 1). Spectra were recorded for each sample in triplicate using 64 scans. The spectra were ATR and automatic baseline corrected and averaged. Peaks were assigned according to the information listed in Table 1. Peak heights were used for comparison.

2.3.2. ^{13}C Nuclear Magnetic Resonance (NMR) Spectroscopy. The ^{13}C CP-MAS NMR spectral analysis was performed on a Bruker DRX 400. Samples were packed in zirconia rotors (5 mm Ø, 160 μL) and spun at 6 kHz using a Chemimagnetics solid state probe (relaxation time 10 ms) and obtained 4096 or

dx.doi.org/10.1021/ie4014259 | Ind. Eng. Chem. Res. 2014, 53, 2940−2955

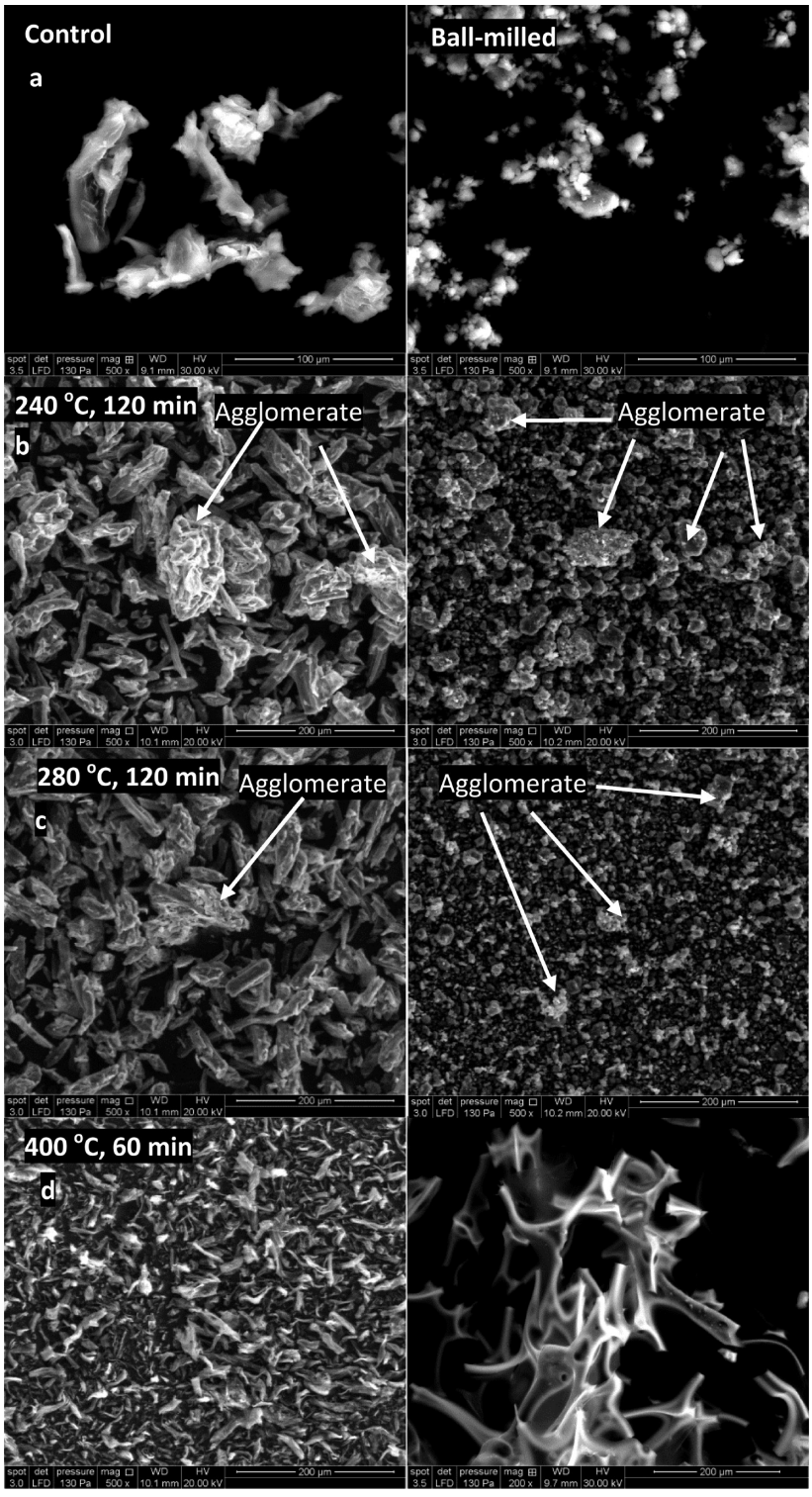

Figure 4. Comparison of control cellulose (left) and ball-milled cellulose (right) (a) and after pyrolysis for 120 min at 240 (b) and 280 °C (c) and for 60 min at 400 °C (d). The melted char of ball-milled cellulose was crushed for sampling.

16 384 scans. This method was utilized to monitor the amount of carbon related to functional groups (aliphatic, aromatic, furanyl, carbonyl, and cellulose related). The spectra were processed using ACD lab software. Peaks were assigned according to previous studies in the literature.[23,54] The area of peaks was evaluated by a deconvolution method applying Guassian and Lorentzian lines previously used in describing cellulose structures.[55−61] The areas of the peaks were considered the molar fraction of the carbon assigned. In this paper, we considered that the aromatic C is in the form of benzene (C_6H_6); that the aliphatic carbon is in the form of methylene ($-CH_2$); that the oligosaccharide carbon is in the form of levoglucosan ($C_6H_{10}O_5$); and the furanyl carbon is in the form of furan (C_4H_4O). On the basis of this supposition, we calculated the mass fraction of each of the functional groups. The mass fraction of the group was then multiplied by the yield

dx.doi.org/10.1021/ie4014259 | Ind. Eng. Chem. Res. 2014, 53, 2940−2955

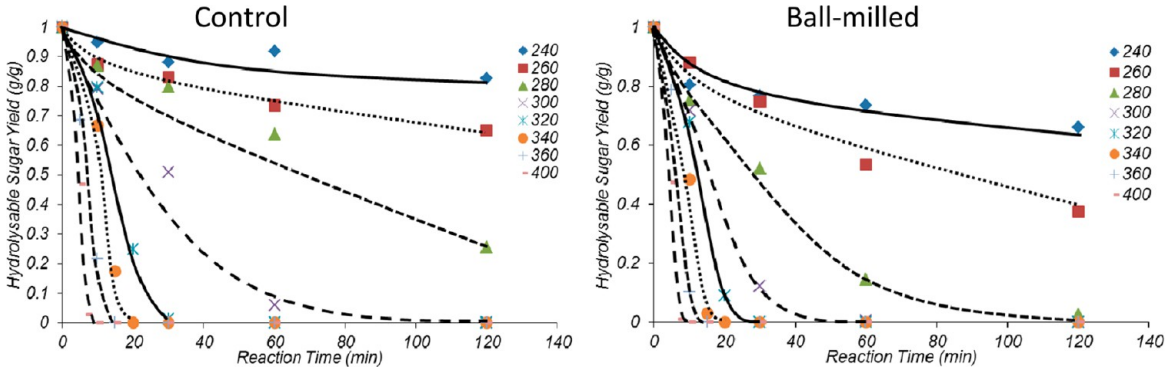

Figure 5. Hydrolyzable sugar content obtained from cellulose residue after pyrolysis as a function of time for (left) control cellulose and (right) ball-milled cellulose. The crystalline cellulose solid residue actually contained more hydrolyzable material than ball-milled cellulose residue after pyrolysis.

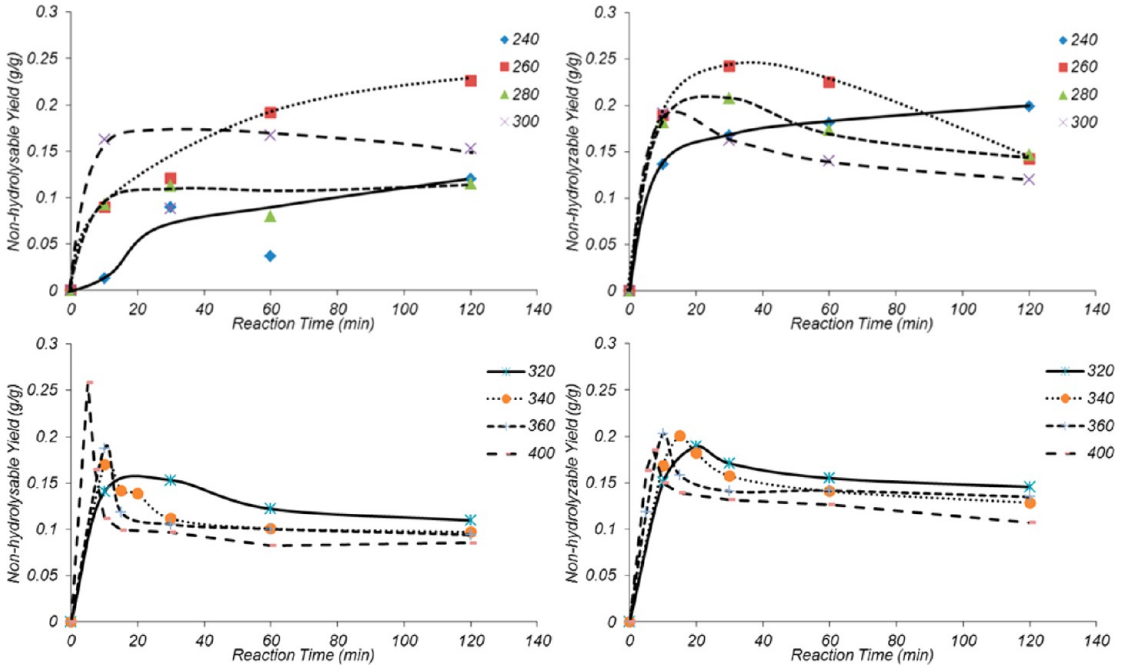

Figure 6. Yield of nonhydrolyzable material (charcoal + cross-linked saccharides) from cellulose ((left) control and (right) ball-milled cellulose) after pyrolysis as a function of reaction time.

of the solid residue to obtain the yield of the group expressed on initial cellulose basis.

2.3.3. Hydrolysis and Ion Exchange Chromatography. The solid samples were hydrolyzed following the ASTM D5896-96 standard.[62] Briefly, approximately 100 mg of sample were weighed in a culture tube (25 mm × 150 mm). One milliliter of 72% H_2SO_4 was added to the tube and mixed with glass rod at 30 °C for 1 h. Then, water (28 mL) was carefully added (to rinse the glass rods) and the tube was sealed and autoclaved (125 °C for 1 h). The hydrolysates were diluted 250 times and filtered for ion exchange chromatographic (IEC, Dionex ICS-3000 Ion Chromatograph, equipped with CarboPac PA20 3 × 150 mm column) analysis. Results collected were multiplied by the yield of residue to reflect the evolution of the solid phase on initial cellulose basis.

2.3.4. SEM (Scanning Electron Microscopy). SEM analyses were performed on an FEI Quanta 200F with a Large Field Detector and a low vacuum of 130 Pa. Samples were distributed evenly (by visual estimation) on adhesive tape on a metal stub.

3. RESULTS AND DISCUSSION

3.1. Yield of Solid Residue. Figure 3 shows the evolution of the solid phase residue and conversion (α) as a function of pyrolysis conditions (time and temperature) for the control and ball-milled cellulose from the spoon reactor described in the Material section. Conversion was calculated as

$$\alpha_{(t)} = (m_{\text{cellulose}(t=0)} - m_{\text{residue}(t)}) / (m_{\text{cellulose}(t=0)} - m_{\text{residue}(t=\infty)}) \quad (1)$$

Control cellulose remained relatively unconverted at temperatures below 260 °C; however, ball-milled cellulose lost approximately 40% of its weight below 260 °C. This difference was also found in our previous study using a thermogravimetric analyzer (TGA), where ball-milled cellulose started its weight loss at lower temperature.[43] A linear relationship was observed at pyrolysis temperatures below 260 °C. The depolymerization of the control cellulose accelerates at 280 °C. Remarkably, this is a huge difference in weight loss in a relatively small temperature regime. At temperatures above 300 °C, both

dx.doi.org/10.1021/ie4014259 | Ind. Eng. Chem. Res. 2014, 53, 2940−2955

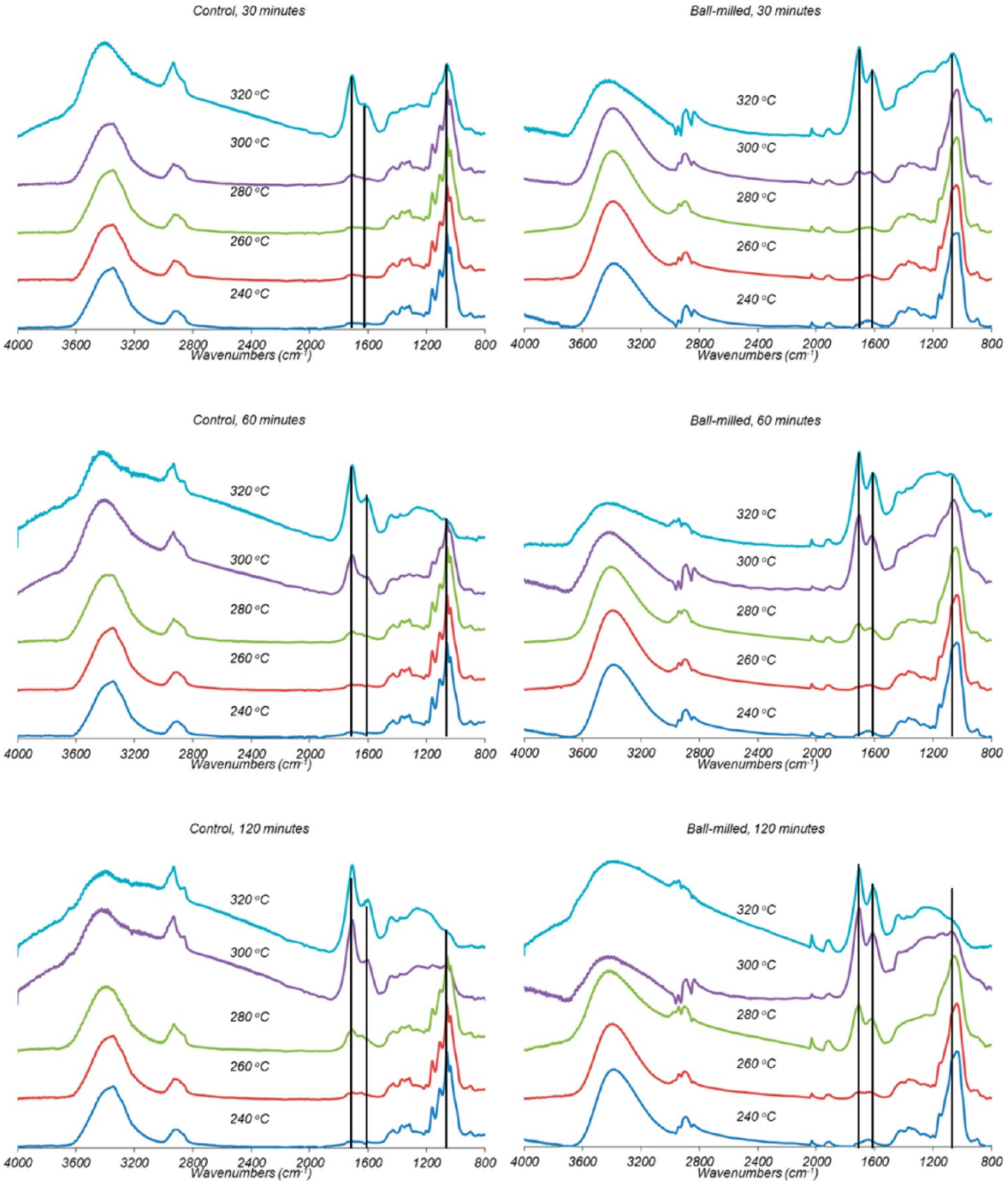

Figure 7. FTIR spectra of pyrolyzed ball-milled cellulose for 30, 60, or 120 min at 240, 260, 280, 300, or 320 °C.

samples reached similar weight losses (>85%) after 30 min of thermal treatment. The weight loss results shown are similar to those of Liu et al.[63] and Pastorova et al.[64]

Pyrolyzed cellulose solids were examined by SEM. Figure 4 shows micrographs of control and ball-milled cellulose at the native state (Figure 4a) and after being treated for 120 min at 240 and 280 and for 60 min at 400 °C (Figure 4b). Large agglomerates were formed from the sticky liquid on the surface of both samples pyrolyzed at 240 °C, even without a large loss of mass. The formation of liquid intermediates evidently occurs at low temperatures. Dufour et al.[65,66] discussed the origin of proton mobility within "a viscous and mobile material" during pyrolysis, which is another way to describe the liquid intermediate. Liu et al.[63] claimed that this material is likely to be water-soluble and composed of anhydro-oligosugars.

Considering the crystallinity of our control cellulose (60%), it is reasonable to assume the amorphous zones of cellulose started to melt at 240 °C. After 120 min at 300 °C, the difference between the control and ball-milled cellulose was more evident (see Figure 3). Although both cellulose samples had a weight loss >50% and shrunk in particle size (see Figure 4c), ball-milled cellulose coalesced after pyrolysis for 120 min. At 320 °C, the ball-milled cellulose samples started to transform into a single piece of char (not shown). Figure 4d reveals that at 400 °C for 60 min, ball-milled cellulose after pyrolysis lost its particle structure and was totally melted; while

dx.doi.org/10.1021/ie4014259 | Ind. Eng. Chem. Res. 2014, 53, 2940−2955

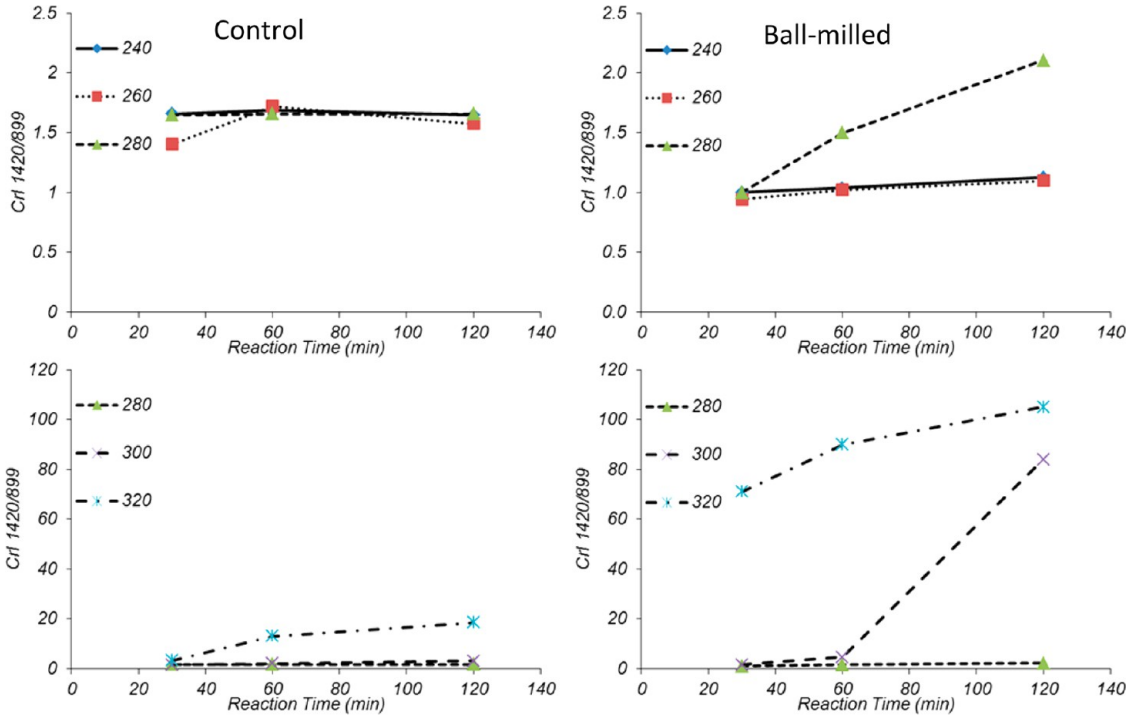

Figure 8. Crystalline cellulose/cellulose ratio (I_{1420}/I_{899}) from FTIR for (left) control and (right) ball-milled cellulose at differing temperatures as a function of reaction time.

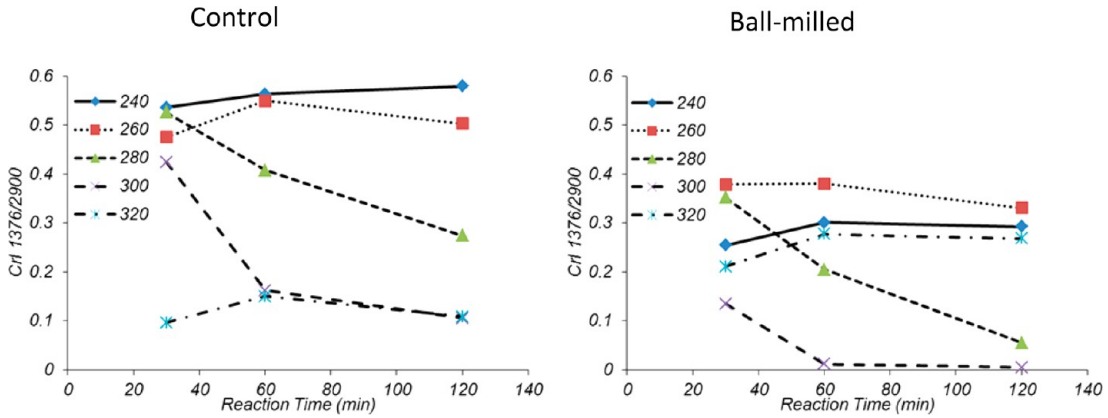

Figure 9. Crystalline cellulose/biomass ratio (I_{1376}/I_{2900}) from FTIR for (left) control and (right) ball-milled cellulose at differing temperatures as a function of reaction time.

the control crystalline cellulose particles indeed shrank, they retained their fibrous structures.

3.2. Quantification of Hydrolyzable Saccharides. Figure 5 shows the content of hydrolyzable sugars remaining in the solid residue, determined by ion exchange chromatography (IEC). The formation of glucose is related to the amount of hydrolyzable saccharides which comes from the nonreacted (original) cellulose. The content of hydrolyzable sugar decreased, following the same trends reported for the weight loss in Figure 3. This result was similar to the results found in earlier works[23,37,64,67] where the hydrolyzable residue decreased as temperature and heating time increased. It also confirmed the formation of a nonhydrolyzable fraction as the pyrolytic conversion of cellulose advances. As the pyrolysis temperature increased, the treated cellulose samples went from yellow to brown and finally to black. When the residual carbonaceous solids were less than 20%, the residue was difficult to hydrolyze.

The yields of nonhydrolyzable material in the various samples are shown in Figure 6 ($m_{\text{nonhydrolyzable}} = m_{\text{solid residue(prehydrolysis)}} - m_{\text{hydrolyzable sugars}}$). The content of nonhydrolyzable saccharides was very pronounced in the early stages of thermal treatment (weight loss < 50%). The nonhydrolyzable material formed from the dehydration, cross-linking, and polycondensation of cellulose and/or cellulose products.[68−70] For example, at 240 °C and 120 min, 20% of ball-milled cellulose is nonhydrolyzable; under the same conditions, only 12% of the control cellulose was nonhydrolyzable. The residue of ball-milled cellulose (~17% in yield) from pyrolysis at 280 °C for 120 min had ~85% nonhydrolyzable saccharides, while the residue of control cellulose (~10% in yield) had ~25% of nonhydrolyzable saccharides.

Ball-milled cellulose shows a reduction in nonhydrolyzable content under less extreme conditions: a higher max yield could

dx.doi.org/10.1021/ie4014259 | Ind. Eng. Chem. Res. 2014, 53, 2940−2955

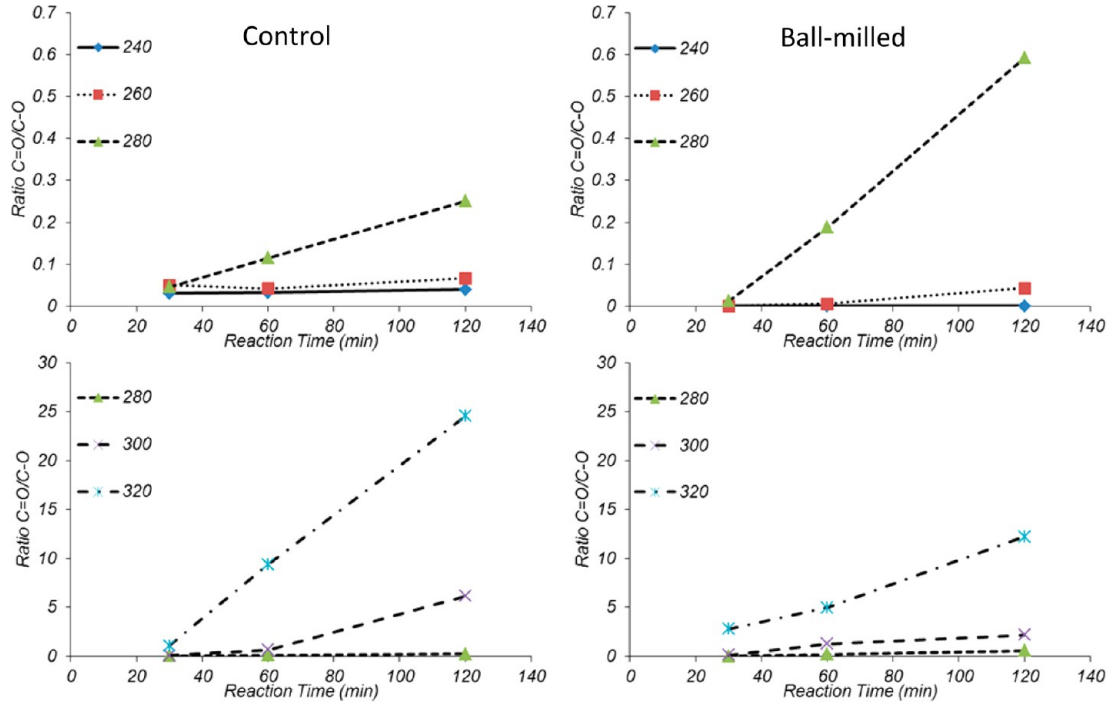

Figure 10. C═O/C—O ratio from FTIR for (left) control and (right) ball-milled cellulose at differing temperatures as a function of reaction time.

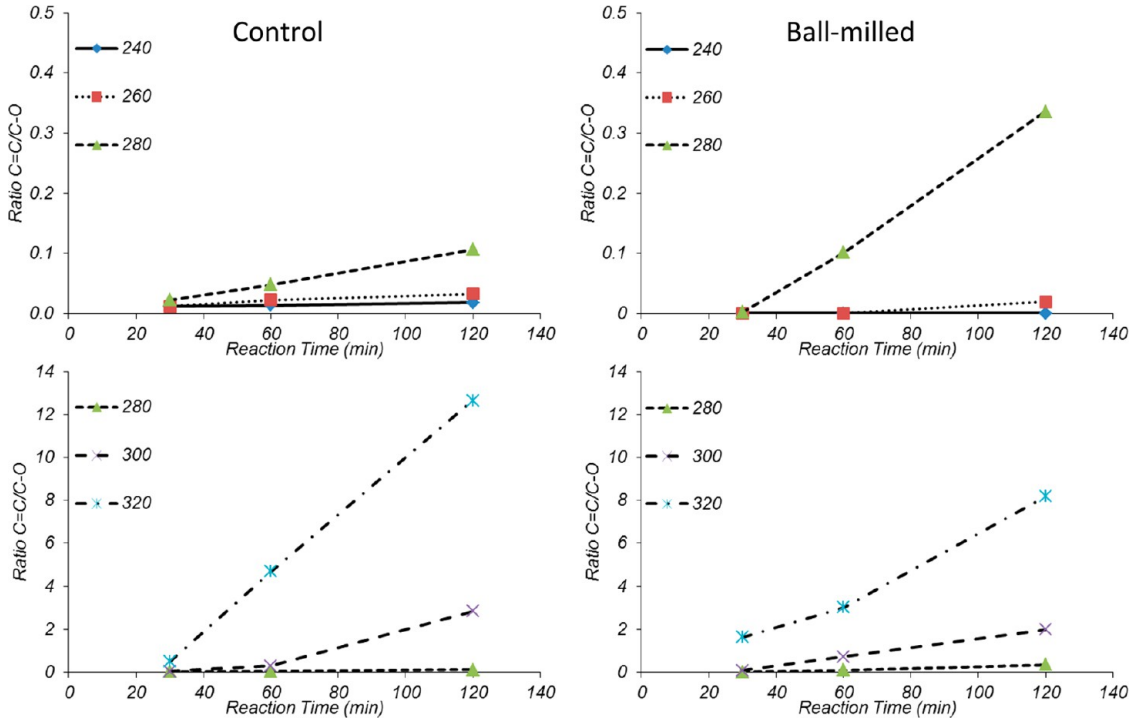

Figure 11. C═C/C—O ratio from FTIR for (left) control and (right) ball-milled cellulose at differing temperatures as a function of reaction time.

be found in ball-milled cellulose until temperatures above 340 °C. This phenomenon may be due to the formation of liquid intermediates that accelerate dehydration and cross-linking reactions.

3.3. FTIR Spectroscopy. Figure 7 shows the FTIR spectra of control and ball-milled cellulose residues obtained after pyrolysis at 240, 260, 280, 300, or 320 °C for 30, 60, or 120 min to qualitatively track the evolution of functional groups in the solid samples. Pyrolysis above 320 °C and 30 min produced black restudies which are unsuitable for analyses on our FTIR setting, so only residues formed at temperatures below 320 °C were analyzed.

Both cellulose samples followed similar trends in their functional group evolution. The structure of cellulose did not change at temperatures below 240 °C. Evidence of cellulose intraring dehydration was indicated by the formation of C═O (1710 cm^{-1}) and C═C (1620 cm^{-1}) bands at temperatures close to 260 °C that increased as the severity (temperature and

dx.doi.org/10.1021/ie4014259 | Ind. Eng. Chem. Res. 2014, 53, 2940−2955

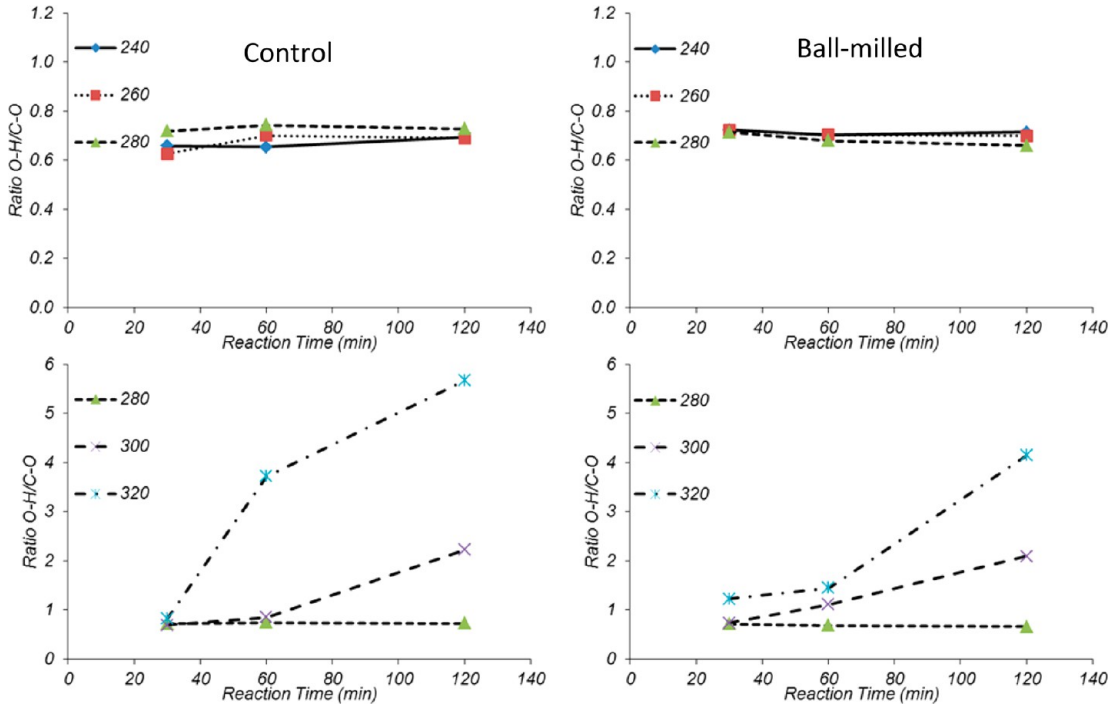

Figure 12. OH/C—O ratio from FTIR for (left) control and (right) ball-milled cellulose at differing temperatures as a function of reaction time.

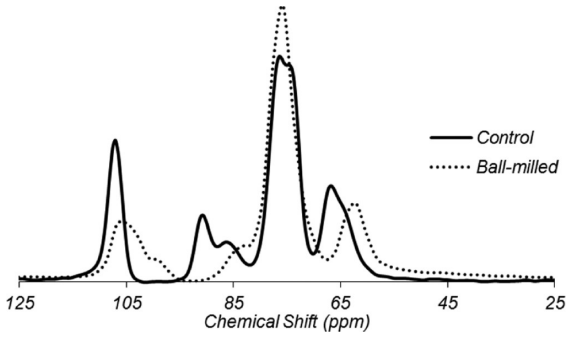

Figure 13. ^{13}C- NMR spectra of control and ball-milled cellulose.

time) increased.[68] Obvious weakening of the C—O band at 1060 cm^{-1} was observed above 280 °C. This C—O band disappeared at 320 °C under 120 min of treatment, indicating that cellulose structure was completely modified under these conditions.

A detailed analysis of the FTIR band height was used to follow changes in chemical characteristics of the solid residue. Figures 8 and 9 show the change of two crystallinity indexes: I_{1420}/I_{892} (in this work, band 892 shifted to 899 cm^{-1}, so here we use I_{1420}/I_{899} to represent this crystallinity index) and I_{1376}/I_{2900} obtained from the FTIR spectra.[71,72] The first index (I_{1420}/I_{899}) shown in Figure 8 is proportional to the ratio of crystalline cellulose to remaining cellulose. The second index (I_{1376}/I_{2900}) shown in Figure 9 is proportional to the ratio of crystalline cellulose to total residue.

Figure 8 shows that the ratio of crystalline cellulose to remaining cellulose decreased for the ball-milled cellulose than the control but increased very rapidly when heated. We saw this result in our previous work,[43] and it clearly suggests that most of the weight loss observed for ball-milled cellulose around 280 °C was due to the conversion of the amorphous cellulose and a concomitant increase in crystalline concentration. Furthermore, Figure 9 shows that the actual content of crystalline cellulose in the residue was initially higher for the control but then decreased with process severity.

Figure 10 shows the ratio between C═O/C—O ($I_{1694-1710}/I_{990-1070}$) for control and ball-milled cellulose. The C═O groups are formed by the intramolecular dehydration reactions.[68] Below 280 °C these reactions seem to be favored in amorphous cellulose, perhaps due to the acceleration of dehydration reactions when the liquid intermediate is formed.[48] It has been explained that dehydration reactions occur via E1-elimination mechanism and are mediated by an acid catalyst.[48] The existence of a melting step at around 280 °C is likely required to form the C═O group for an intraring dehydration environment. The formation of agglomerates in this range of temperature is a clear indication of the presence of liquid intermediates on the surface of the converted cellulose particles.

At higher temperatures the dehydration reactions are more, pronounced as seen by the dramatic increase in C═O/C—O. The evolution of the C═C/C—O ratio ($I_{1597-1620}/I_{990-1070}$) can be seen in Figure 11. The trends observed for the C═C/C—O were very similar to that observed for the C═O/C—O ratio both of which are products of intraring dehydration reactions. At higher temperatures the solid residue formed from the control cellulose seems to have higher content of C═C groups.

Figure 12 shows the OH/C—O ratio ($I_{3100-3600}/I_{990-1070}$) for control and ball-milled cellulose. This ratio did not change significantly below 300 °C and was very similar for both the control and ball-milled samples. This ratio dramatically increased above 300 °C, indicating the dehydration of hydroxyl group at C-3 (1060 cm^{-1}) and C-6 (1030 cm^{-1}) positions on the native glucopyranose ring.

3.4. ^{13}C NMR Spectroscopy. Solid state CP-MAS ^{13}C NMR spectroscopy was used to monitor C functional groups in cellulose. Figure 13 shows the difference between control and ball-milled cellulose. Spectra for control cellulose is consistent

dx.doi.org/10.1021/ie4014259 | Ind. Eng. Chem. Res. 2014, 53, 2940−2955

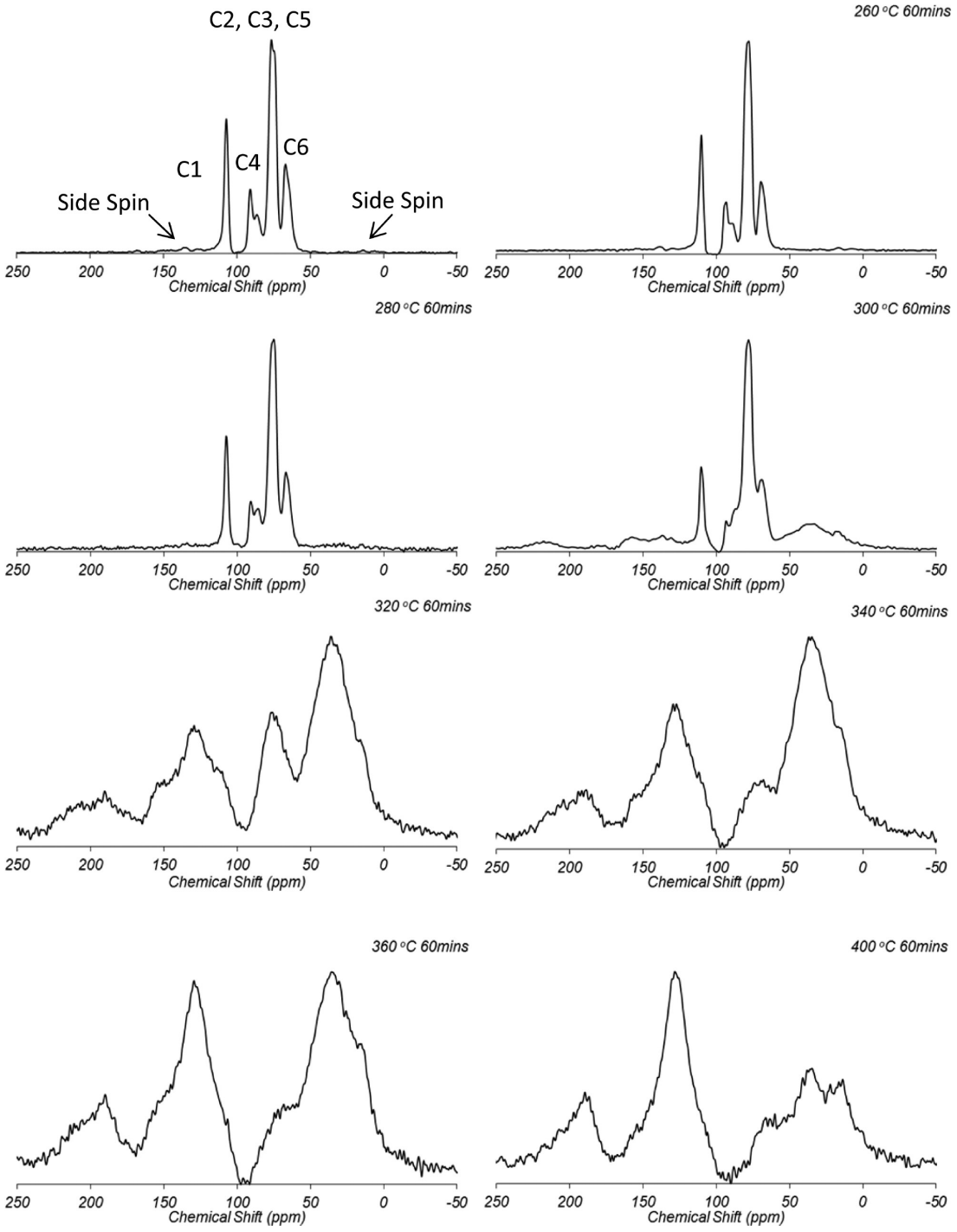

Figure 14. ^{13}C NMR spectra for pyrolyzed control cellulose at differing conditions.

with those reported by Pastorova et al.[23] C-6 at ~66 ppm (62 ppm for ball-milled); C-2, C-3, C-5 at 74–76 (doublet) ppm (75 ppm for ball-milled); anomeric C-1 peak at 107 ppm (104 ppm for ball-milled); C-4 at 90 (crystalline) and 86 (amorphous) ppm (85 ppm for ball-milled).

Figure 14 shows the evolution of ^{13}C NMR as a function of pyrolysis conditions. The ^{13}C spectra were peak fitted following the method described for cellulose crystallinity and allomorph analysis, modified to accommodate the thermally derived structures after pyrolysis.[55−61] The molar fraction of C associated to the different structures was calculated from the mass fraction of all the functional groups (aromatics, aliphatic, carbohydrate, and furanyl) and multiplied by the yield of solid residue to obtain the functional group yield on initial cellulose basis. The results of carbohydrate, aliphatic, and aromatic were plotted in Figure 15.

The content of the carbohydrates decreased gradually following a trend similar to that measured by acid hydrolysis. Aliphatic groups were formed faster in ball-milled cellulose above 300 °C. At 300 °C, control cellulose products showed a higher presence of aliphatic groups than for ball-milled cellulose. Above 300 °C, trends were similar. Aromatic groups were formed more rapidly in the ball-milled samples than the control samples. The formation of aromatic groups is mainly

dx.doi.org/10.1021/ie4014259 | Ind. Eng. Chem. Res. 2014, 53, 2940−2955

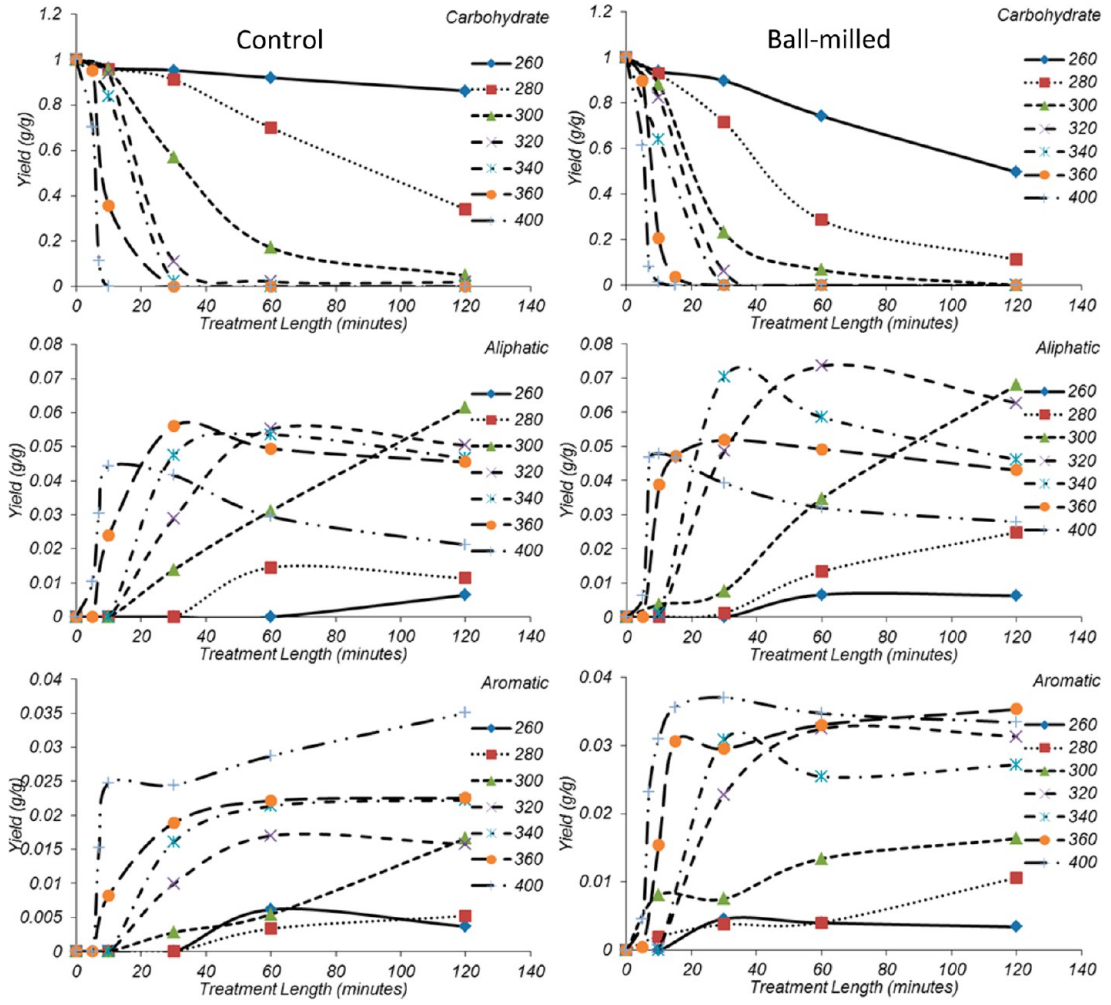

Figure 15. Graph showing the yield of carbohydrate, aliphatic, and aromatic groups for (left) control and (right) ball-milled cellulose at differing pyrolysis temperatures as a function of reaction time.

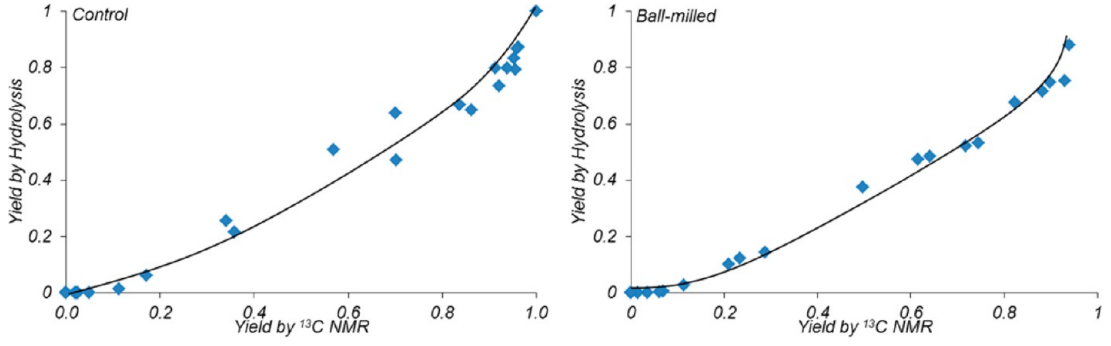

Figure 16. Comparison of cellulose content determined by hydrolysis and ^{13}C NMR.

due to aromatization and polycondensation reactions responsible for charcoal formation. These groups seem to be stable in the conditions studied.

Figure 16 shows a correlation between the cellulose content measured by acid hydrolysis to that determined by quantitative ^{13}C NMR. The values of cellulose determined by acid hydrolysis were lower than those determined by ^{13}C NMR. It means that the ^{13}C NMR quantification method used, accounted the very poorly quantified cross-linked saccharides as carbonhydrate (cellulose).

Figure 17 shows the evolution of furanyl and carbonyl groups as a function of pyrolysis conditions. The furanyl and carbonyl groups are products of dehydration reactions. Similar to results from Py-GC/MS reported elsewhere,[43] higher yields of these two groups were formed in the ball-milled cellulose. This may be attributed to the more facile formation of liquid intermediates from amorphous cellulose.

It is important to note that the addition of aliphatic, aromatic, furanyl, and carboxyl fractions was considerably lower that the content of nonhydrolyzable saccharides shown in Figure 6. This

dx.doi.org/10.1021/ie4014259 | Ind. Eng. Chem. Res. 2014, 53, 2940−2955

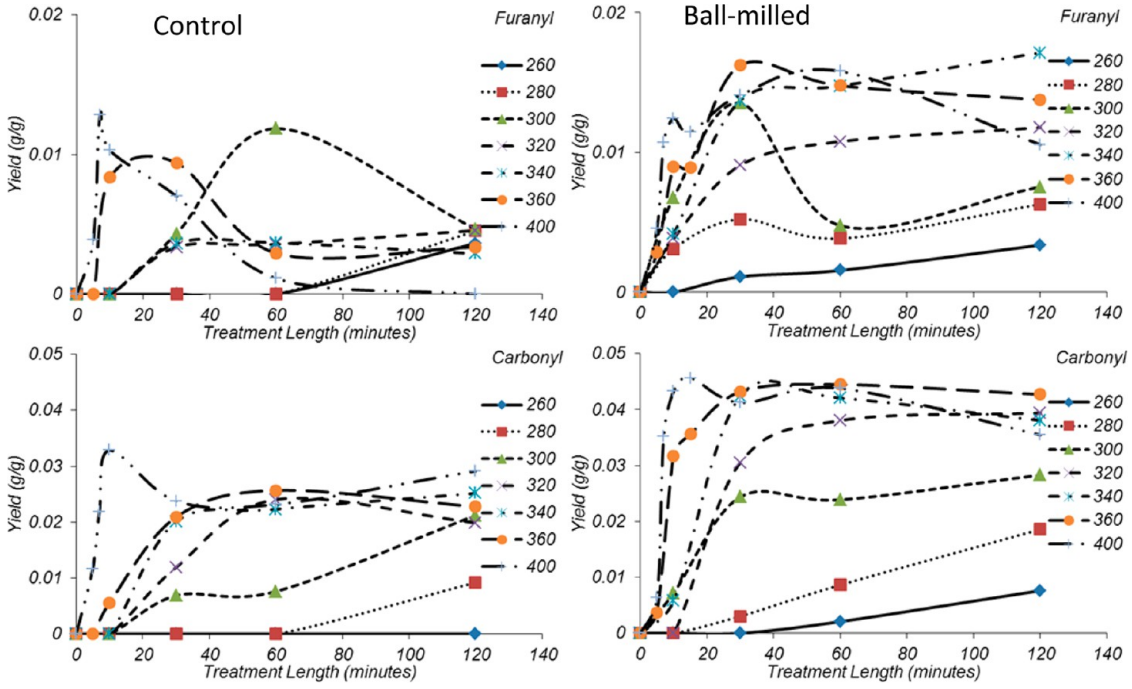

Figure 17. Yield of furanyl and carbonyl groups for (left) control and (right) ball-milled cellulose at differing pyrolysis temperatures as a function of reaction time.

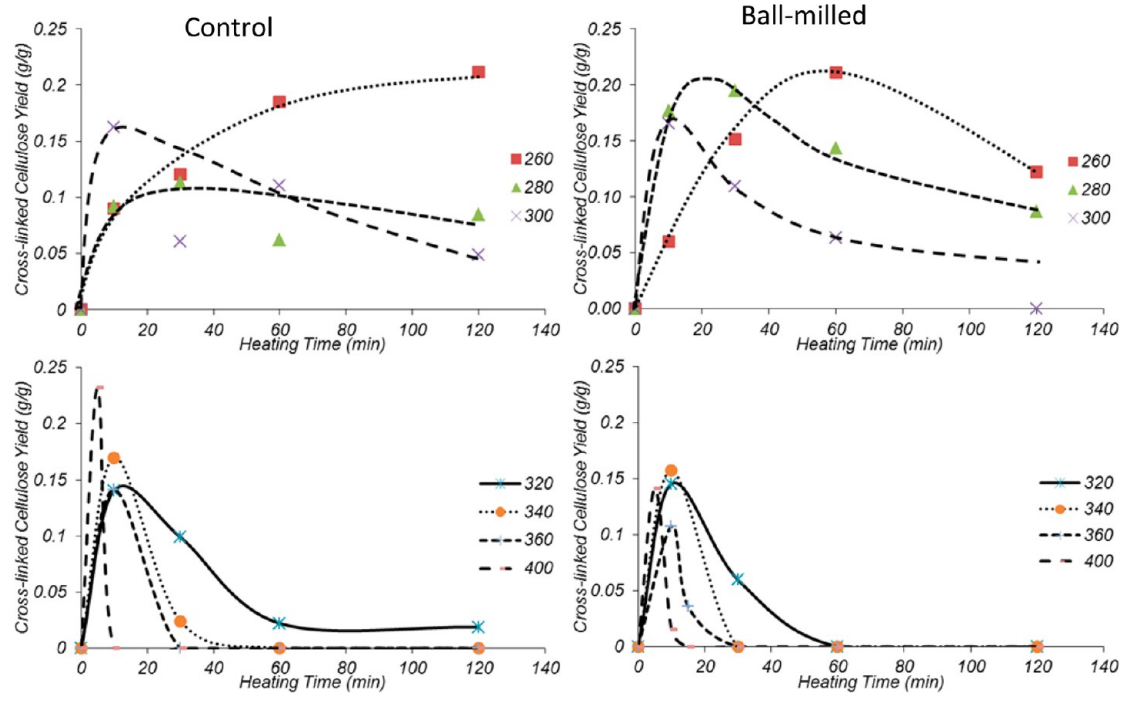

Figure 18. Behavior of nonhydrolyzable cross-linked saccharides.

difference clearly indicates that the ^{13}C NMR method accounted for the modified cross-linked saccharides as cellulose.

The difference between the cellulose content measured by ^{13}C NMR and the cellulose content measured by acid hydrolysis is an estimate for the yield of cross-linked sugars. The same results are obtained if the yields of furanyl, carbonyl, aliphatic, and aromatic are subtracted from the yield of nonhydrolyzable sugars. The yields of cross-linked saccharides are shown in Figure 18. In conclusion, the ^{13}C NMR results indicate that the cross-linked saccharides are formed through ether bonds from various yet-to-be-determined hydroxyl groups.

3.5. Reaction Mechanism. The data presented in Figures 5 and 15−18 were used to develop a new reaction mechanism explaining the behavior of cellulose during slow/intermediate pyrolysis conditions (see Figure 19). The authors recognize that the experimental data obtained with an initial heating period between 2 and 10 min does not allow obtaining real "kinetic" constants using methods developed for isothermal systems. Experiments under very high heating/mass transfer

dx.doi.org/10.1021/ie4014259 | Ind. Eng. Chem. Res. 2014, 53, 2940−2955

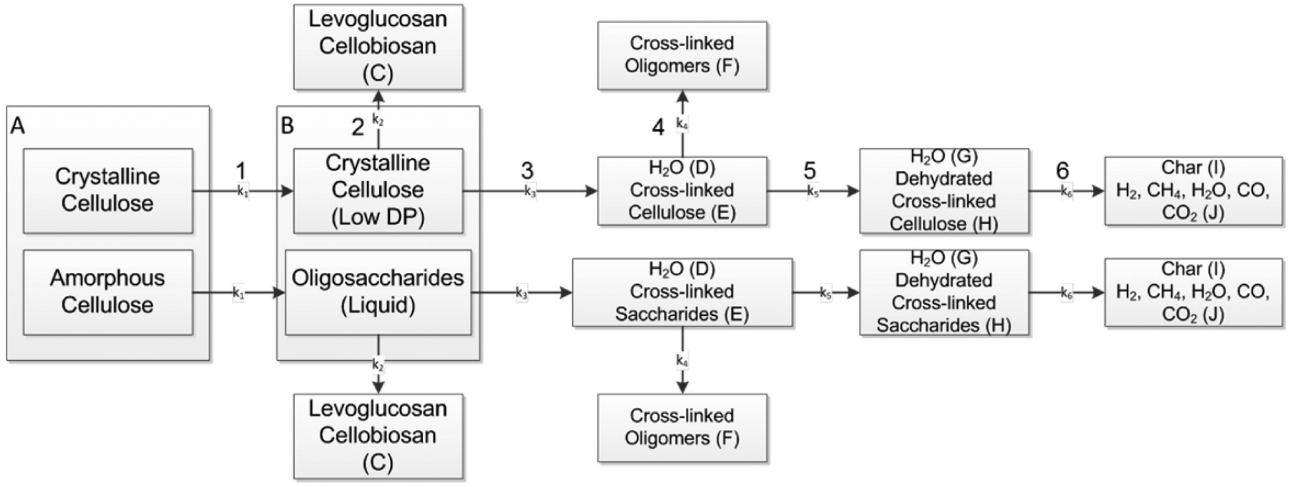

Figure 19. Reaction mechanism proposed for cellulose slow pyrolysis.

rates, and rapid product quenching conditions will have to be conducted to find the kinetic parameters of the reactions in the mechanism proposed.

The first reaction (**1**) describes the early stage depolymerization of cellulose (A) to produce a low Dp cellulose (B). The basic unit of crystalline cellulose morphology is the elementary fibril (a nanocrystal) with approximately 300 Angstrom surrounded by amorphous zones that can be easily broken at low temperature (150−190 °C).[73] The formation of a nanocrystal with molecular weight close to 300−400 g/mol when crystalline cellulose is heated has been reported by Shafizadeh.[74] The amorphous zones can be depolymerized all the way to produce oligomeric liquid intermediates. This cellulose with low Dp has the same formula as cellulose ($C_6H_{10}O_5$). This step does not lead to any weight loss.

The second reaction (**2**) is associated with the further depolymerization of low Dp cellulose to produce volatile anhydro-, mono-, and oligo-saccharides (chiefly levoglucosan and cellobiosan) (C). This reaction causes weight losses and has been extensively studied in the literature.[75−79] It consists of glycosidic bond cleavages at the ends of cellulose polymer chains. Once this reaction is initiated, the whole chain "unzips" to release monomers of levoglucosan and dimers of cellobiosan.[75−78,80−82] The evaporation of levoglucosan and other potential liquid intermediates has been extensively studied by Oja and Suuberg.[50]

The third reaction (**3**) corresponds to inter-ring dehydration responsible for the formation of water and cross-linked saccharides.[48,68−70] Inter-ring dehydration of the low Dp cellulose (B) releases one unit of water (D) from every two glucopyranose bound together and gives a cross-linked saccharide complex (E) with a basic unit of $C_6H_9O_{4.5}$. While Mamleev et al.[48] argued this reaction is associated with the formation of liquid intermediate, Chaiwat et al.[69,70] presented their mechanism supposing a solid phase reaction. The existence of cellulose-derived liquid intermediates has been confirmed by our SEM studies. This liquid intermediate seems to be formed by products of cellulose depolymerization (levoglucosan, cellobiosan, cellotriosan, etc.) and their cross-linking products which are not volatile enough to evaporate.[27,50,69,70,83]

The fourth reaction (**4**) is the cracking of cross-linked structures to form volatile products (F), extensively studied by Chaiwat et al.[69,70]

The fifth reaction (**5**) describes the ring contraction and dehydration of cross-linked saccharides, as studied by Scheirs et al.[68] The dehydration of group E releases one unit of water (G) for every basic unit to form a cross-linked saccharide complex H ($C_6H_7O_{3.5}$).

The sixth reaction (**6**) represents the polycondensation of dehydrated saccharides (H) to form char (I). This reaction has been poorly studied in the literature.[23,51] According to Shafizadeh and Sekiguchi[84] and McGrath et al.,[85] the product can be represented by the formula ($C_5H_{3.5}O$). The water and gases (J) produced in this reaction are contained in the formula ($CH_{3.5}O_{2.5}$).

4. CONCLUSION

A spoon reactor was used to compare pyrolytic solids from ball-milled amorphous and microcrystalline cellulose. Below 260 °C, only the ball-milled cellulose presented significant weight losses. The microcrystalline cellulose underwent major weight loss at 280 °C. At temperatures over 300 °C, both samples showed similar weight loss. This result was also found in our previous study under TGA, where ball-milled cellulose started its weight loss at lower temperature.[43]

Ball-milled cellulose enhanced the liquid intermediate phase during pyrolysis. Nonhydrolyzable oligosaccharides were formed in both the ball-milled and microcrystalline cellulose but disappeared as temperature increased. This suggests that inter-ring dehydration and cross-linking reactions are favored in liquid intermediates. Ball-milled cellulose formed these compounds at lower temperatures more so than microcrystalline cellulose. Carbohydrates disappear faster, aliphatics form faster, and aromatics form faster in the ball-milled than control cellulose up to 300 °C. Higher yields of furanyl and carbonyl groups were observed in the ball-milled cellulose than control.

On the basis of this knowledge, a new reaction scheme was presented with six reactions that for the first time explicitly includes the formation of cross-linked (nonhydrolyzable) cellulose and its further depolymerization to produce non-hydrolyzable saccharides.

AUTHOR INFORMATION

Corresponding Author

*Telephone: 509-335-7758. Fax: 509-335-2722. E-mail: mgarcia-perez@wsu.edu.

Notes

The authors declare no competing financial interest.

■ ACKNOWLEDGMENTS

This project was financially supported by the US National Science Foundation (CBET-0966419, CAREER CBET-1150430), the Sun-Grant Initiative (Interagency Agreement: T0013G-A), and the Washington State Agricultural Research Center. The authors are very thankful for their support.

■ REFERENCES

(1) Berndes, G.; Hoogwijk, M.; van den Broek, R. The contribution of biomass in the future global energy supply: a review of 17 studies. *Biomass Bioenergy* **2003**, *25* (1), 1−28.
(2) Huber, G. W.; Iborra, S.; Corma, A. Synthesis of transportation fuels from biomass: chemistry, catalysts, and engineering. *Chem. Rev.* **2006**, *106*, 4044−4098.
(3) Kheshgi, H. S.; Prince, R. C.; Marland, G. The potential of biomass fuels in the context of global climate change: Focus on Transportation Fuels1. *Ann. Rev. Energy Environ.* **2000**, *25* (1), 199−244.
(4) Elliott, D. C.; Beckman, D.; Bridgwater, A. V.; Diebold, J. P.; Gevert, S. B.; Solantausta, Y. Developments in direct thermochemical liquefaction of biomass: 1983−1990. *Energy Fuels* **1991**, *5* (3), 399−410.
(5) Grange, P.; Laurent, E.; Maggi, R.; Centeno, A.; Delmon, B. Hydrotreatment of pyrolysis oils from biomass: reactivity of the various categories of oxygenated compounds and preliminary techno-economical study. *Catal. Today* **1996**, *29* (1−4), 297−301.
(6) Bridgwater, A. V. Production of high grade fuels and chemicals from catalytic pyrolysis of biomass. *Catal. Today* **1996**, *29* (1−4), 285−295.
(7) Sjöström, E. *Wood chemistry: fundamentals and applications*; Academic Press Inc., 1993.
(8) Kersten, S.; Garcia-Perez, M. Recent developments in fast pyrolysis of ligno-cellulosic materials. *Curr. Opin. Biotechnol.* **2013**, *24* (3), 414−420.
(9) Essig, M.; Richards, G. N.; Schenck, E. M. Mechanisms of formation of the major volatile products from the pyrolysis of cellulose. In *Cellulose and Wood Chemistry and Technology*; Schuerch, C., Ed.; John Wiley & Sons: New York, 1989.
(10) Lowary, T. L.; Richards, G. N. Mechanisms of pyrolysis of polysaccharides: cellobiitol as a model for cellulose. *Carbohydrate Res.* **1990**, *198* (1), 79−89.
(11) Ponder, G. R.; Qiu, H.-X.; Richards, G. N. Pyrolytic conversion of biomass to anhydrosugars. *Appl. Biochem. Biotechnol.* **1990**, *24* (1), 41−47.
(12) Richards, G. N.; Zheng, G. Influence of metal ions and of salts on products from pyrolysis of wood: applications to thermochemical processing of newsprint and biomass. *J. Anal. Appl. Pyrol.* **1991**, *21* (1), 133−146.
(13) Lian, J.; Chen, S.; Zhou, S.; Wang, Z.; O'Fallon, J.; Li, C.-Z.; Garcia-Perez, M. Separation, hydrolysis and fermentation of pyrolytic sugars to produce ethanol and lipids. *Bioresour. Technol.* **2010**, *101* (24), 9688−9699.
(14) Lian, J.; Garcia-Perez, M.; Chen, S. Fermentation of levoglucosan with oleaginous yeasts for lipid production. *Bioresour. Technol.* **2013**, *133* (0), 183−189.
(15) Molton, P. M.; Demmitt, T. F. *Reaction mechanisms in cellulose pyrolysis: a literature review*; Battelle Pacific Northwest Laboratories, 1977; BNWL-2297.
(16) Arseneau, D. F. Competitive reactions in the thermal decomposition of cellulose. *Can. J. Chem.* **1971**, *49* (4), 632−638.
(17) Lin, Y.-C.; Cho, J.; Tompsett, G. A.; Westmoreland, P. R.; Huber, G. W. Kinetics and Mechanism of Cellulose Pyrolysis. *J. Phys. Chem. C* **2009**, *113* (46), 20097−20107.
(18) Milosavljevic, I.; Suuberg, E. M. Cellulose Thermal Decomposition Kinetics: Global Mass Loss Kinetics. *Ind. Eng. Chem. Res.* **1995**, *34* (4), 1081−1091.
(19) Shafizadeh, F.; Bradbury, A. G. W. Thermal degradation of cellulose in air and nitrogen at low temperatures. *J. Appl. Polym. Sci.* **1979**, *23* (5), 1431−1442.
(20) Bradbury, A. G.; Sakai, Y.; Shafizadeh, F. A kinetic model for pyrolysis of cellulose. *J. Appl. Polym. Sci.* **1979**, *23* (11), 3271−3280.
(21) Varhegyi, G.; Antal, M. J.; Szekely, T.; Szabo, P. Kinetics of the thermal decomposition of cellulose, hemicellulose, and sugarcane bagasse. *Energy Fuels* **1989**, *3* (3), 329−335.
(22) Shafizadeh, F.; Fu, Y. L. Pyrolysis of cellulose. *Carbohydr. Res.* **1973**, *29* (1), 113−122.
(23) Pastorova, I.; Botto, R. E.; Arisz, P. W.; Boon, J. J. Cellulose char structure: a combined analytical Py-GC-MS, FTIR, and NMR study. *Carbohydr. Res.* **1994**, *262* (1), 27−47.
(24) Broido, A.; Nelson, M. A. Char yield on pyrolysis of cellulose. *Combust. Flame* **1975**, *24* (0), 263−268.
(25) Piskorz, J.; Radlein, D. S. A. G.; Scott, D. S.; Czernik, S. Pretreatment of wood and cellulose for production of sugars by fast pyrolysis. *J. Anal. Appl. Pyrol.* **1989**, *16* (2), 127−142.
(26) Diebold, J. P. A unified, global model for the pyrolysis of cellulose. *Biomass Bioenergy* **1994**, *7* (1−6), 75−85.
(27) Wooten, J. B.; Seeman, J. I.; Hajaligol, M. R. Observation and Characterization of Cellulose Pyrolysis Intermediates by 13C CPMAS NMR. A New Mechanistic Model. *Energy Fuels* **2003**, *18* (1), 1−15.
(28) Varhegyi, G.; Jakab, E.; Antal, M. J. Is the Broido-Shafizadeh Model for Cellulose Pyrolysis True? *Energy Fuels* **1994**, *8* (6), 1345−1352.
(29) Várhegyi, G.; Antal, M. J., Jr; Jakab, E.; Szabó, P. Kinetic modeling of biomass pyrolysis. *J. Anal. Appl. Pyrol.* **1997**, *42* (1), 73−87.
(30) Westerhof, R. J. M.; Brilman, D. W. F.; Garcia-Perez, M.; Wang, Z.; Oudenhoven, S. R. G.; Kersten, S. R. A. Stepwise Fast Pyrolysis of Pine Wood. *Energy Fuels* **2012**, *26* (12), 7263−7273.
(31) Lewellen, P. C.; Peters, W. A.; Howard, J. B. Cellulose pyrolysis kinetics and char formation mechanism. *Symp. (Int.) Combustion* **1977**, *16* (1), 1471−1480.
(32) Dobele, G.; Meier, D.; Faix, O.; Radtke, S.; Rossinskaja, G.; Telysheva, G. Volatile products of catalytic flash pyrolysis of celluloses. *J. Anal. Appl. Pyrol.* **2001**, *58*−*59* (0), 453−463.
(33) Basch, A.; Lewin, M. The influence of fine structure on the pyrolysis of cellulose. I. Vacuum pyrolysis. *J. Polym. Sci.: Polym. Chem. Ed.* **1973**, *11* (12), 3071−3093.
(34) Broido, A.; Weinstein, M. Thermogravimetric Analysis of Ammonia-Swelled Cellulose. *Combust. Sci. Technol.* **1970**, *1* (4), 279−285.
(35) Weinstetn, M.; Broido, A. Pyrolysis-Crystallinity Relationships in Cellulose. *Combust. Sci. Technol.* **1970**, *1* (4), 287−292.
(36) Antal, M. J., Jr. Biomass pyrolysis: a review of the literature part 1—carbohydrate pyrolysis. In *Advances in solar energy*; Springer, 1985; pp 61−111.
(37) Patai, S.; Halpern, Y. Pyrolytic Reaction of Carbohydrates. Part IX. The Effect of Additives on the Thermal Behavior of Cellulose Samples of Different Crystallinity. *Isr. J. Chem.* **1970**, *8*, 655.
(38) Halpern, Y.; Patai, S. Pyrolytic reactions of carbohydrates. Part VI. Isothermal decomposition of cellulose in vacuo, in the presence of additives. *Isr. J. Chem.* **1969**, *7*, 685−690.
(39) Halpern, Y.; Patai, S. Pyrolytic reactions of carbohydrates. Part V. Isothermal decomposition of cellulose in vacuo. *Isr. J. Chem.* **1969**, *7*, 673−683.
(40) Kilzer, F. J.; Broido, A. Speculations on the nature of cellulose pyrolysis. *Pyrodynamics* **1965**, *2* (2), 151−163.
(41) Shimazu, F.; Sterling, C. Effect of wet and dry heat on structure of cellulose. *J. Food Sci.* **1966**, *31* (4), 548−551.
(42) Kato, K.; Komorita, H. Pyrolysis of Cellulose Part IV. Effect of Crystallinity of Cellulose on the Formation of the Volatile Compounds. *Agric. Biol. Chem.* **1968**, *32* (1), 21−26.

(43) Wang, Z.; McDonald, A. G.; Westerhof, R. J. M.; Kersten, S. R. A.; Cuba-Torres, C. M.; Ha, S.; Pecha, B.; Garcia-Perez, M. Effect of cellulose crystallinity on the formation of a liquid intermediate and on product distribution during pyrolysis. *J. Anal. Appl. Pyrol.* **2013**, *100* (0), 56−66.
(44) Antal, M., Jr. Biomass Pyrolysis: A Review of the Literature Part 2—Lignocellulose Pyrolysis. In *Advances in Solar Energy*; Böer, K., Duffie, J., Eds.; Springer, 1985; pp 175−255.
(45) Boutin, O.; Ferrer, M.; Lédé, J. Radiant flash pyrolysis of cellulose—Evidence for the formation of short life time intermediate liquid species. *J. Anal. Appl. Pyrol.* **1998**, *47* (1), 13−31.
(46) Lédé, J.; Diebold, J. P.; Peacocke, G. V. C.; Piskorz, J., The nature and properties of intermediate and unvaporized biomass pyrolysis materials. In *Developments in Thermochemical Biomass Conversion*; Bridgwater, A. V., Boocock, D. G. B., Eds.; 1997; Vol. *1*, pp 27−42.
(47) Dauenhauer, P. J.; Colby, J. L.; Balonek, C. M.; Suszynski, W. J.; Schmidt, L. D. Reactive boiling of cellulose for integrated catalysis through an intermediate liquid. *Green Chem.* **2009**, *11* (10), 1555−1561.
(48) Mamleev, V.; Bourbigot, S.; Le Bras, M.; Yvon, J. The facts and hypotheses relating to the phenomenological model of cellulose pyrolysis: Interdependence of the steps. *J. Anal. Appl. Pyrol.* **2009**, *84* (1), 1−17.
(49) Feng, W.; van der Kooi, H. J.; de Swaan Arons, J. Application of the SAFT equation of state to biomass fast pyrolysis liquid. *Chem. Eng. Sci.* **2005**, *60* (3), 617−624.
(50) Oja, V.; Suuberg, E. M. Vapor Pressures and Enthalpies of Sublimation of d-Glucose, d-Xylose, Cellobiose, and Levoglucosan. *J. Chem. Eng. Data* **1998**, *44* (1), 26−29.
(51) Kawamoto, H.; Murayama, M.; Saka, S. Pyrolysis behavior of levoglucosan as an intermediate in cellulose pyrolysis: polymerization into polysaccharide as a key reaction to carbonized product formation. *J. Wood Sci.* **2003**, *49* (5), 469−473.
(52) Teixeira, A. R.; Mooney, K. G.; Kruger, J. S.; Williams, C. L.; Suszynski, W. J.; Schmidt, L. D.; Schmidt, D. P.; Dauenhauer, P. J. Aerosol generation by reactive boiling ejection of molten cellulose. *Energy Environ. Sci.* **2011**, *4* (10), 4306−4321.
(53) Mauviel, G.; Kies, F.; Rene, M. S.; Ferrer, M.; Lede, J. Attrition-free pyrolysis to produce bio-oil and char. *Bioresour. Technol.* **2009**, *100* (23), 6069−75.
(54) Liitiä, T.; Maunu, S. L.; Hortling, B. Solid state NMR studies on cellulose crystallinity in fines and bulk fibres separated from refined kraft pulp. *Holzforschung* **2000**, *54* (6), 618−624.
(55) Heux, L.; Dinand, E.; Vignon, M. R. Structural aspects in ultrathin cellulose microfibrils followed by 13C CP-MAS NMR. *Carbohydr. Polym.* **1999**, *40* (2), 115−124.
(56) Hult, E. L.; Larsson, P. T.; Iversen, T. A comparative CP/MAS 13C-NMR study of cellulose structure in spruce wood and kraft pulp. *Cellulose* **2000**, *7*, 35−55.
(57) Kennedy, C.; Cameron, G.; Šturcová, A.; Apperley, D.; Altaner, C.; Wess, T.; Jarvis, M. Microfibril diameter in celery collenchyma cellulose: X-ray scattering and NMR evidence. *Cellulose* **2007**, *14* (3), 235−246.
(58) Larsson, P. T.; Westermark, U.; Iversen, T. Determination of the cellulose Iα allomorph content in a tunicate cellulose by CP/MAS 13C-NMR spectroscopy. *Carbohydr. Res.* **1995**, *278* (2), 339−343.
(59) Pu, Y.; Ziemer, C.; Ragauskas, A. J. CP/MAS 13C NMR analysis of cellulase treated bleached softwood kraft pulp. *Carbohydr. Res.* **2006**, *341* (5), 591−597.
(60) Wickholm, K.; Larsson, P. T.; Iversen, T. Assignment of non-crystalline forms in cellulose I by CP/MAS 13C NMR spectroscopy. *Carbohydr. Res.* **1998**, *312* (3), 123−129.
(61) Yamamoto, H.; Horii, F. CPMAS carbon-13 NMR analysis of the crystal transformation induced for Valonia cellulose by annealing at high temperatures. *Macromolecules* **1993**, *26* (6), 1313−1317.
(62) *ASTM Standard D5896-96, Standard Test Method for Carbohydrate Distribution of Cellulosic Materials*; ASTM International: West Conshohocken, PA, 2007.
(63) Liu, D.; Yu, Y.; Wu, H. Differences in Water-Soluble Intermediates from Slow Pyrolysis of Amorphous and Crystalline Cellulose. *Energy Fuels* **2013**, *27* (3), 1371−1380.
(64) Pastorova, I.; Arisz, P. W.; Boon, J. J. Preservation of D-glucose-oligosaccharides in cellulose chars. *Carbohydr. Res.* **1993**, *248*, 151−165.
(65) Dufour, A.; Castro-Diaz, M.; Brosse, N.; Bouroukba, M.; Snape, C. The Origin of Molecular Mobility During Biomass Pyrolysis as Revealed by In situ 1H NMR Spectroscopy. *ChemSusChem* **2012**, *5* (7), 1258−1265.
(66) Dufour, A.; Castro-Díaz, M.; Marchal, P.; Brosse, N.; Olcese, R.; Bouroukba, M.; Snape, C. In Situ Analysis of Biomass Pyrolysis by High Temperature Rheology in Relations with 1H NMR. *Energy Fuels* **2012**, *26* (10), 6432−6441.
(67) Boon, J. J.; Pastorova, I.; Botto, R.; Arisz, P. Structural studies on cellulose pyrolysis and cellulose chars by PYMS, PYGCMS, FTIR, NMR and by wet chemical techniques. *Biomass Bioenergy* **1994**, *7* (1), 25−32.
(68) Scheirs, J.; Camino, G.; Tumiatti, W. Overview of water evolution during the thermal degradation of cellulose. *Eur. Polym. J.* **2001**, *37* (5), 933−942.
(69) Chaiwat, W.; Hasegawa, I.; Tani, T.; Sunagawa, K.; Mae, K. Analysis of Cross-Linking Behavior during Pyrolysis of Cellulose for Elucidating Reaction Pathway. *Energy Fuels* **2009**, *23* (12), 5765−5772.
(70) Chaiwat, W.; Hasegawa, I.; Kori, J.; Mae, K. Examination of Degree of Cross-Linking for Cellulose Precursors Pretreated with Acid/Hot Water at Low Temperature. *Ind. Eng. Chem. Res.* **2008**, *47* (16), 5948−5956.
(71) Liang, C. Y.; Marchessault, R. H. Infrared spectra of crystalline polysaccharides. II. Native celluloses in the region from 640 to 1700 cm.−1. *J. Polym. Sci.* **1959**, *39* (135), 269−278.
(72) Nelson, M. L.; O'Connor, R. T. Relation of certain infrared bands to cellulose crystallinity and crystal lattice type. Part II. A new infrared ratio for estimation of crystallinity in celluloses I and II. *J. Appl. Polym. Sci.* **1964**, *8* (3), 1325−1341.
(73) Moon, R. J.; Martini, A.; Nairn, J.; Simonsen, J.; Youngblood, J. Cellulose nanomaterials review: structure, properties and nanocomposites. *Chem. Soc. Rev.* **2011**, *40* (7), 3941−3994.
(74) Shafizadeh, F. Introduction to pyrolysis of biomass. *J. Anal. Appl. Pyrol.* **1982**, *3* (4), 283−305.
(75) Mayes, H. B.; Broadbelt, L. J. Unraveling the Reactions that Unravel Cellulose. *J. Phys. Chem. A* **2012**, *116* (26), 7098−7106.
(76) Piskorz, J.; Radlein, D.; Scott, D. S. On the mechanism of the rapid pyrolysis of cellulose. *J. Anal. Appl. Pyrol.* **1986**, *9* (2), 121−137.
(77) Radlein, D.; Piskorz, J.; Scott, D. S. Fast pyrolysis of natural polysaccharides as a potential industrial process. *J. Anal. Appl. Pyrol.* **1991**, *19* (0), 41−63.
(78) Evans, R. J.; Milne, T. A. Molecular characterization of the pyrolysis of biomass. 2. Applications. *Energy Fuels* **1987**, *1* (4), 311−319.
(79) Vinu, R.; Broadbelt, L. J. A mechanistic model of fast pyrolysis of glucose-based carbohydrates to predict bio-oil composition. *Energy Environ. Sci.* **2012**, *5* (12), 9808−9826.
(80) Shafizadeh, F.; Stevenson, T. T. Saccharification of douglas-fir wood by a combination of prehydrolysis and pyrolysis. *J. Appl. Polym. Sci.* **1982**, *27* (12), 4577−4585.
(81) Golova, O. P. Chemical Effects of Heat on Cellulose. *Russ. Chem. Rev.* **1975**, *44* (8), 687.
(82) Agarwal, V.; Dauenhauer, P. J.; Huber, G. W.; Auerbach, S. M. Ab Initio Dynamics of Cellulose Pyrolysis: Nascent Decomposition Pathways at 327 and 600° C. *J. Am. Chem. Soc.* **2012**, *134* (36), 14958−14972.
(83) Lédé, J. Cellulose pyrolysis kinetics: An historical review on the existence and role of intermediate active cellulose. *J. Anal. Appl. Pyrol.* **2012**, *94*, 17−32.
(84) Shafizadeh, F.; Sekiguchi, Y. Development of aromaticity in cellulosic chars. *Carbon* **1983**, *21* (5), 511−516.

(85) McGrath, T. E.; Chan, W. G.; Hajaligol, M. R. Low temperature mechanism for the formation of polycyclic aromatic hydrocarbons from the pyrolysis of cellulose. *J. Anal. Appl. Pyrol.* **2003**, *66* (1−2), 51−70.